Lithuanian Journal of Physics, Vol. **57**, No. 4, pp. 243–251 (2017)

STRUCTURAL AND ELECTRICAL PROPERTIES OF ARGYRODITE-TYPE Cu_7PS_6 CRYSTALS

I.P. Studenyak [a], V.Yu. Izai [a], A.I. Pogodin [a], O.P. Kokhan [a], V.I. Sidey [a], M.Yu. Sabov [a], A. Kežionis [b], T. Šalkus [b], and J. Banys [b]

[a] *Uzhhorod National University, 46 Pidhirna Str., 88000 Uzhhorod, Ukraine*
[b] *Faculty of Physics, Vilnius University, Saulėtekio 9/3, 10222 Vilnius, Lithuania*
Email: tomas.salkus@ff.vu.lt

Received 16 June 2017; revised 14 July 2017; accepted 20 September 2017

Cu_7PS_6 crystals were grown using direct crystallisation from the melt (Bridgman–Stockbarger technique). The crystal structure of Cu_7PS_6 was determined by X-ray powder diffraction. Cu_7PS_6 crystallise in the cubic structure, space group $P2_13$ (No. 198), the lattice parameter $a = 9.6706(1)$ Å, formula units per cell $Z = 4$. Electrical properties of Cu_7PS_6 crystals were studied in the frequency range 10–10^{10} Hz and in the temperature interval 296–351 K. The performed analysis shows that the Cu_7PS_6 crystals are mixed electron-ionic conductors with some growth defects.

Keywords: inorganic materials, crystal growth, crystal structure, X-ray diffraction, charge transport

PACS: 81.10.-h, 84.37.+q, 61.05.cp

1. Introduction

Cu_7PS_6 compounds belong to argyrodite-type solid electrolytes [1]. The most investigated in this family are Cu_6PS_5I crystals, showing a high value of electric conductivity at room temperature, comparable with the conductivity of the best solid electrolytes [2]. At room temperature Cu_6PS_5I crystals belong to the cubic crystal system ($F\bar{4}3m$ space group) [1]. At low temperatures Cu_6PS_5I crystals undergo two phase transitions (PTs), one of them being a second-order structural PT at $T_{II} = (269 \pm 2)$ K, and the other being a first-order superionic and ferroelastic PT at $T_I = (144–169)$ K [3, 4].

To our knowledge, no detailed studies of the crystal structure of Cu_7PS_6 have been carried out so far. However, the X-ray diffraction analysis of the crystal structure of a similar Cu_7PSe_6 compound has been reported [5]. In the high-temperature phase (above the first-order PT at $T = 320$ K) Cu_7PSe_6 compounds crystallise in the cubic crystal system, space group $F\bar{4}3m$. In the intermediate phase at room temperature Cu_7PSe_6 also crystallise in the cubic crystal system, but in the $P2_13$ space group. Partial ordering of Cu^+ cations is observed at the PT that correlates with the most probable density of states in the high-temperature phase. In the Cu_7PSe_6 argyrodite structure one can mark out $[PSe_6]$ structural elements where Cu^+ cations can occupy linearly, trigonally or tetragonally coordinated positions. Polycrystalline Cu_7PSe_6 argyrodite undergoes a structural phase transition from the orthorhombic $Pna2_1$ space group to the simple cubic $P2_13$ space group near 250 K. In addition, the compound transforms from the $P2_13$ structure to the face-centred cubic $F\bar{4}3m$ structure near 325 K from a partially cation-ordered to a fully disordered high-temperature phase with an increasing amount of mobile copper ions [6].

The electrical studies of Cu_7PSe_6 argyrodite have shown a remarkably high room temperature total conductivity value of 0.4 S/cm (40 S/m), over 90% of the value attributable to an electronic component of conductivity [6]. At the same time one can observe an increase of the mobile cations content above room temperature. A huge degree of disorder in the structure of Cu_7PSe_6, which is correlated to the ionic conducting nature of this compound, leads to trapping of electronic states at the Fermi energy. Thus, holes

were found to be the major charge carriers resulting from intrinsic defects [6].

The activation energy of the conductivity of polycrystalline Cu_7PSe_6 is 0.22 eV in both the low temperature $Pna2_1$ structure ($T < 251$ K) and in the room temperature $P2_13$ structure (251 K < T < 322 K). The activation energy drops slightly to a value of 0.17 eV in the high temperature $F\bar{4}3m$ structure ($T > 322$ K) [6]. At temperatures from 425 to 575 K the calculated activation energy of 0.28 eV reported in work [7] was larger than the value of 0.17 eV for the high temperature modification reported by Beeken et al. earlier [8]. In the temperature region between 325 and 425 K the temperature dependent electrical resistivity of polycrystalline Cu_7PSe_6 shows a strong decrease of electrical resistivity, related to the abovementioned phase transition [5–8].

In comparison with the isomorphous analogue Cu_7PSe_6, the physical properties of which are presented above, unfortunately, the physical properties of the Cu_7PS_6 compound have been studied insufficiently. The phase diagram of the quasibinary Cu_2S–P_4S_{10} system was studied in Ref. [9]. The Cu_7PS_6 compound is formed with a large excess of S^{2-} anions and in a simplified case its structure can be viewed as a Cu_2S matrix containing isolated $[PS_4]^{3-}$ ions [9]. Its high-temperature modification contains a disordered subsystem of metal ions that are characterised by high ionic conductivity due to a considerable mobility of monovalent cations while during cooling an ordered phase is formed [9]. In Cu_7PS_6 a PT is observed at 515 K from the high-temperature phase with $F\bar{4}3m$ symmetry to the low-temperature phase with $P2_13$ symmetry. Calorimetric studies of Cu_7PS_6 showed no phase transitions in the temperature range 100–400 K, the linear temperature dependence of specific heat capacity being an evidence for strong anharmonicity [10].

Therefore, a detailed investigation of the structural and electrical properties of the Cu_7PS_6 argyrodite-type superionic conductor is of great interest. The present paper is aimed at development of the growth technology and studies of the crystal structure as well as the electrical conductivity of Cu_7PS_6 crystals.

2. Materials and methods

Cu_7PS_6 single crystals were grown using direct crystallisation from the melt (Bridgman–Stockbarger technique). Synthesis of the Cu_7PS_6 compound was performed in the following way: heating at a rate of 50 K/h to 673 ± 5 K, ageing at this temperature for 24 h, then heating to 973 ± 5 K, ageing at this temperature for 72 h, further heating of the melting zone up to 1380 ± 5 K that is by 50 K above the melting temperature with 24 h ageing. The ageing resulted in nucleation. Annealing of the formed seeds was performed for 48 h. The growth rate was kept at 3 mm/day. The annealing zone temperature was 973 ± 5 K, and the annealing duration was 48 h. As a result, Cu_7PS_6 crystals with a length of 45–50 mm and 10–2 mm in diameter were obtained.

The crystal structure of Cu_7PS_6 was determined using the X-ray diffraction (XRD) technique. The X-ray powder diffraction data for Cu_7PS_6 were collected using a *Stoe* Stadi P diffractometer (transmission geometry, germanium-monochromated Cu Kα_1 radiation, $\lambda = 1.5406$ Å, $2\theta = 2.000$–$92.030°$, step $\Delta 2\theta = 0.015°$, room temperature) equipped with a *Mythen* 1K detector.

Measurements of the complex impedance ($\tilde{Z}$) of Cu_7PS_6 single crystals were carried out in the frequency range 10–10^{10} Hz in the temperature interval 296–351 K using a coaxial impedance spectrometer [11, 12]. A sample was prepared from the Cu_7PS_6 single crystal in the shape of a cylinder with the height $h = 2.25$ mm and the base surface area $A = 2.54$ mm^2. Silver was used for the preparation of electrodes. Further on we are presenting the intrinsic electrical parameters of the Cu_7PS_6 crystal: complex resistivity

$$\tilde{\rho} = \tilde{Z}\frac{A}{h}, \tag{1}$$

complex conductivity

$$\tilde{\sigma} = 1/\tilde{\rho} \tag{2}$$

and complex dielectric permittivity

$$\tilde{\varepsilon} = j\frac{\tilde{\sigma}}{\omega}, \tag{3}$$

where $j^2 = -1$ and $\omega = 2\pi f$ is the angular frequency.

3. Results and discussion

Preliminary analyses (autoindexing, space group determination, and basic Rietveld refinement [13, 14] procedures) of the powder diffraction pattern obtained for Cu_7PS_6 were performed using

the *EXPO2014* software [15]. These analyses have clearly shown that Cu_7PS_6 crystallises in the cubic β-Cu_7PSe_6 [5] structure type, space group $P2_13$ (No. 198), lattice parameter $a = 9.6706(1)$ Å, formula units per cell $Z = 4$. Attempts to refine the crystal structure of Cu_7PS_6 in other structural models reported for argyrodite [1] structures of similar stoichiometry and of the same space group [16, 17] resulted in much poorer fit-quality indicators.

Final Rietveld refinement procedures [13, 14] were performed using the *FullProf.2k* software [18]. The Pearson VII [19] function was used for simulation of the peak shape. Intensities within 32 times of the full width at half maximum (FWHM) were considered to contribute to the reflection. The background was modelled using the Fourier filtering technique. The peaks below 60° (2θ) were corrected for asymmetry effects by using the Bérar–Baldinozzi model [20]. The effect of the preferred orientation along the [110] direction was corrected using the March–Dollase model [21]. Due to strong mutual correlations between certain refinable parameters in the least squares refinement procedures, individual atomic displacement ("thermal") parameters could not be reliably determined; hence, at the final refinement stages, these parameters were constrained to be equal for all copper atoms and for all sulfur atoms in the structure, whereas the displacement parameter for the phosphorus atom was fixed.

The refinement converged with the profile residuals $R_p = 4.66\%$ and $R_{wp} = 6.53\%$, and with the intensity residual (the so-called "Bragg *R*-factor") $R_B = 3.00\%$. While the R_p and R_{wp} values are critically dependent on the background level of powder diffraction patterns and, therefore, cannot serve as the fit-quality markers [22], the quite low R_B value (which is *not* affected by the background level) obtained here clearly indicates a reasonable agreement between the experimental data and the theoretical structural model for Cu_7PS_6 ternary sulfide.

The experimental details and crystallographic data for Cu_7PS_6 at room temperature are collected in Table 1; the atomic coordinates, isotropic displacement ("thermal") parameters and site occupancy factors (SOFs) of the Cu_7PS_6 crystal structure are given in Table 2; the selected interatomic

Table 1. Experimental details and crystallographic data for Cu_7PS_6.

Crystal system; space group	Cubic; $P2_13$ (No. 198)
Lattice parameter	$a = 9.6706(1)$ Å
Cell volume	$V = 904.39(1)$ Å^3
Chemical formula weight	FW = 668.15
Formula units per cell	$Z = 4$
Calculated density	$D_c = 4.907$ g/cm^3
Temperature of data collection	$T = 293(2)$ K
Radiation type; wavelength	Cu Kα_1; $\lambda = 1.5406$ Å
Powder diffractometer; geometry	Stoe Stadi P; transmission
Monochromator	Ge(1 1 1)
2θ scan range; step	2.000–92.030°; 0.015°
2θ refinement range	9.500–92.030°
Refinement programme	*FullProf.2k*
Peak shape function	Pearson VII
Peak asymmetry function	Bérar–Baldinozzi
Background treatment	Fourier filtering (window of 3000 datapoints)
Preferred orientation model; direction	March–Dollase; [1 1 0]
Number of atom sites	9
Number of free structural parameters	21
Total number of free parameters	33
Profile *R*-factors	$R_p = 4.66\%$; $R_{wp} = 6.53\%$
Bragg *R*-factor	$R_B = 3.00\%$
Goodness of fit	$\chi^2 = 1.06$

Table 2. Atomic coordinates, isotropic displacement parameters (B_{iso} values) and site occupancy factors (SOFs) for the Cu_7PS_6 crystal structure.

Atom	Position	*x/a*	*y/b*	*z/c*	B_{iso} (Å^2)	SOF
P	4a	0.7426(9)	0.7426(9)	0.7426(9)	0.3a	1
S1	4a	0.8683(12)	0.8683(12)	0.8683(12)	0.45(9)	1
S2	12b	0.3610(7)	0.3724(8)	0.8805(9)	0.45(9)	1
S3	4a	0.2304(7)	0.2304(7)	0.2304(7)	0.45(9)	1
S4	4a	0.4919(9)	0.4919(9)	0.4919(9)	0.45(9)	1
Cu1	12b	0.0753(6)	–0.0945(5)	–0.2623(4)	2.12(8)	1
Cu2	12b	0.0023(16)	0.0017(22)	0.2789(8)	2.12(8)	0.63(2)
Cu3	12b	0.0375(27)	0.0557(33)	0.2750(16)	2.12(8)	0.37(2)
Cu4	4a	0.3650(8)	0.3650(8)	0.3650(8)	2.12(8)	1

[a] is a fixed parameter.

distances are given in Table 3. Figure 1 illustrates the most important part of the final Rietveld plot for the Cu_7PS_6 compound.

The crystal structure of the Cu_7PS_6 ternary sulfide belongs to a large family of the argyrodite structures [17] and contains a cation–anion coordination shell of four different types: [PS_4], [CuS_4], [CuS_3], and [CuS_2] (see Table 3 and Fig. 2). The main difference of the β-Cu_7PSe_6 [16] structure type (in which the Cu_7PS_6 compound is crystallised) from other argyrodite models of similar stoichiometry and of the same space group [18, 19] is the split position of a copper atom, resulting in two 12b positions (Cu2 and Cu3) with partial site occupancies (see Table 2).

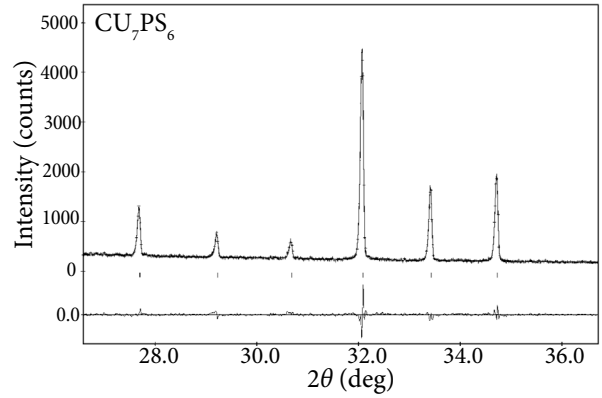

Fig. 1. Fragment of the final Rietveld plot for Cu_7PS_6: experimental (crosses), theoretical (a solid line), and difference (a solid line in the bottom) powder XRD patterns. Reflection positions are marked by vertical bars.

Table 3. Selected interatomic distances (Å) for the Cu_7PS_6 crystal structure.

[PS_4] coordination shell	
P–S1	2.105(15)
P–S2 (×3)	1.999(12)
[CuS_4] coordination shells	
Cu1–S1	2.394(13)
Cu1–S2	2.441(9)
Cu1–S3	2.294(9)
Cu1–S4	2.562(10)
Cu3–S2	2.37(3)
Cu3–S2	2.49(3)
Cu3–S3	2.56(3)
Cu3–S4	2.342(19)

[CuS_3] coordination shell	
Cu2–S2	2.391(16)
Cu2–S2′	2.299(17)
Cu2–S4	2.220(12)
[CuS_2] coordination shell	
Cu4–S3	2.255(10)
Cu4–S4	2.126(12)
Shortest Cu–Cu contacts	
Cu1–Cu2	2.728(12)
Cu1–Cu2′	2.825(13)
Cu1–Cu3	2.34(2)
Cu1–Cu4	2.948(9)
Cu2–Cu3	0.62(3)
Cu2–Cu3′	2.88(3)

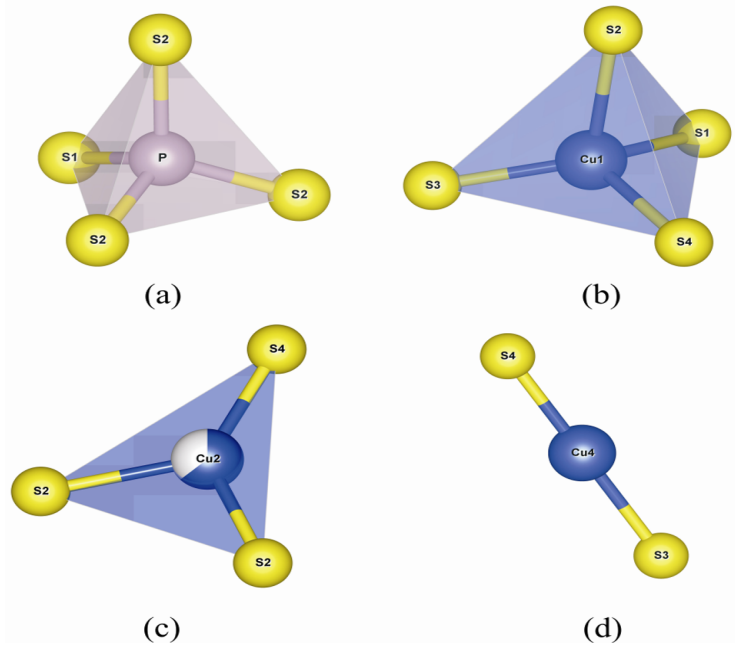

Fig. 2. Coordination shells in the Cu_7PS_6 crystal structure: (a) $[PS_4]$, (b) $[CuS_4]$, (c) $[CuS_3]$, and (d) $[CuS_2]$.

As with other argyrodite structures [17], anions (sulfur atoms) in the crystal structure of Cu_7PS_6 form a framework built of interpenetrating centred icosahedra. Figure 3 shows a typical icosahedron formed by sulfur atoms in the Cu_7PS_6 crystal structure.

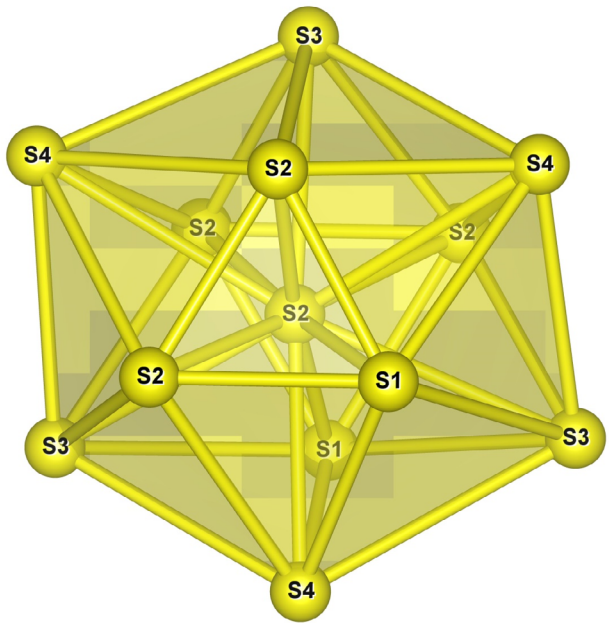

Fig. 3. An icosahedron formed by sulfur atoms in the Cu_7PS_6 crystal structure.

The frequency dependences of the electric properties measured at different temperatures are presented in Fig. 4. Two relaxation processes were found in the spectra of Cu_7PS_6 crystal electric properties. The conductivity dispersion regions are related to these processes. The first one is observed in the frequency range from about 10 kHz up to about 100 MHz, while the other dispersion was found above 3 GHz frequency (Fig. 4(a)). Both dispersions reveal themselves as maxima of the complex resistivity imaginary part (Fig. 4(b)). The maximum of the imaginary part of complex resistivity corresponds to relaxation frequency, which increases with the increase of temperature. In the frequency range from about 10 MHz up to 1 GHz a well-defined dispersion of dielectric permittivity was found, while in the frequency ranges below 10 MHz and above 1 GHz dielectric permittivity decreases slightly with the increase of frequency (see Fig. 4(c)). Temperature dependences of the real part of dielectric permittivity measured at 4 GHz frequency are shown in the inset of Fig. 4(c). A gradual decrease of ε' from 26.3 to 23 was observed in the studied temperature range.

In Fig. 5 resistivity is presented in the complex plane plot. In this case each relaxation is represented by a semicircle. Similarly to the Cole–Cole expression used to describe dielectric permittivity, the complex resistivity can be written as

$$\tilde{\rho} = \rho_b + \frac{\Delta\rho}{1+(j\omega\tau)^{1-\alpha}}, \tag{4}$$

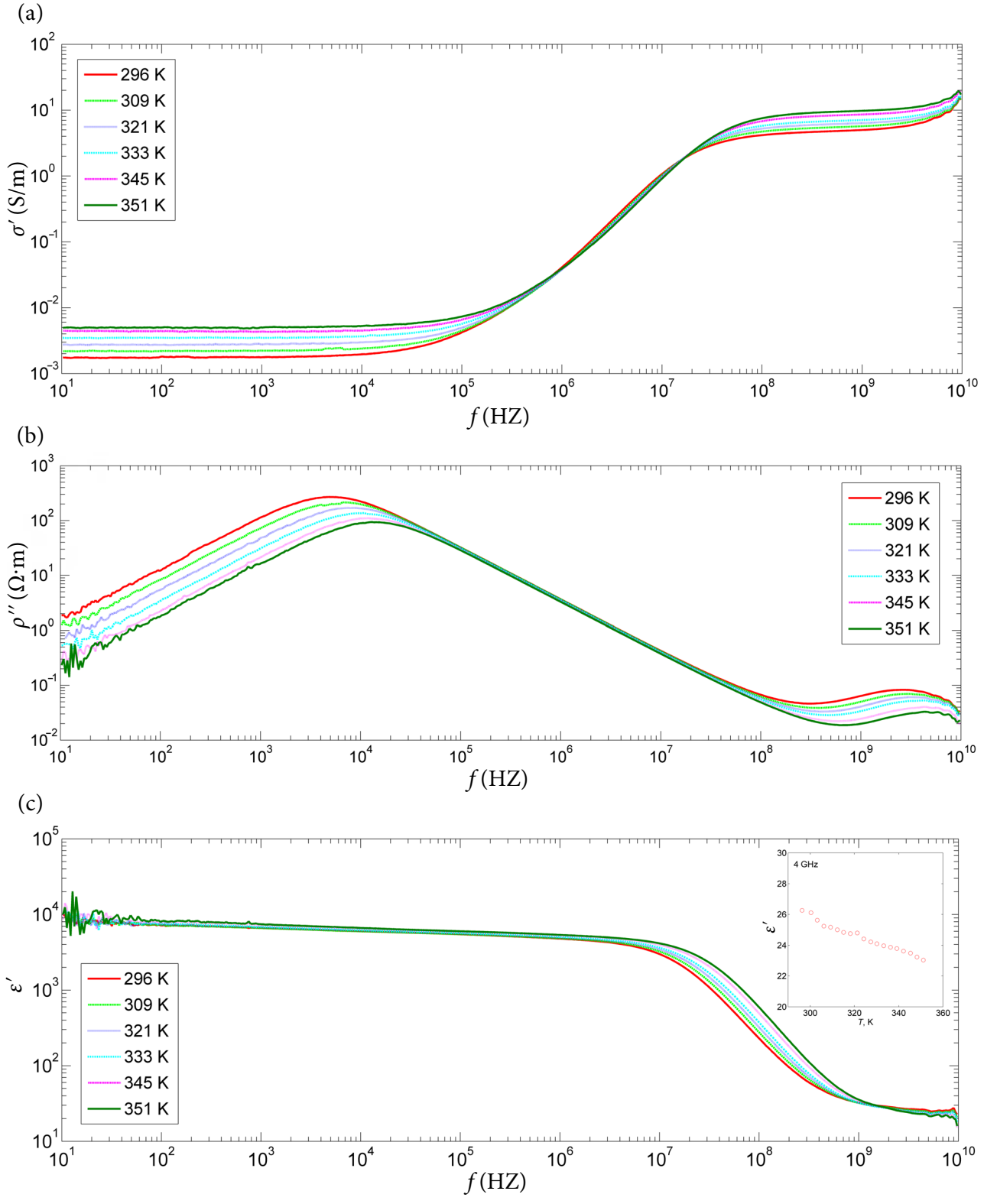

Fig. 4. Frequency dependences of the real part of complex conductivity (a), the imaginary part of complex resistivity (b), and the real part of complex dielectric permittivity (c) measured at different temperatures (coloured online).

where $\Delta\rho$ is the diameter of a semicircle, ρ_b is the point where the semicircle intersects with the real axis, τ is the relaxation time and α is a parameter describing the distribution of relaxation times. As could be expected for a single crystal, the relaxations in the Cu_7PS_6 crystal are almost of Debye-type, and the values of the parameter α = 0.97 were obtained for both relaxations.

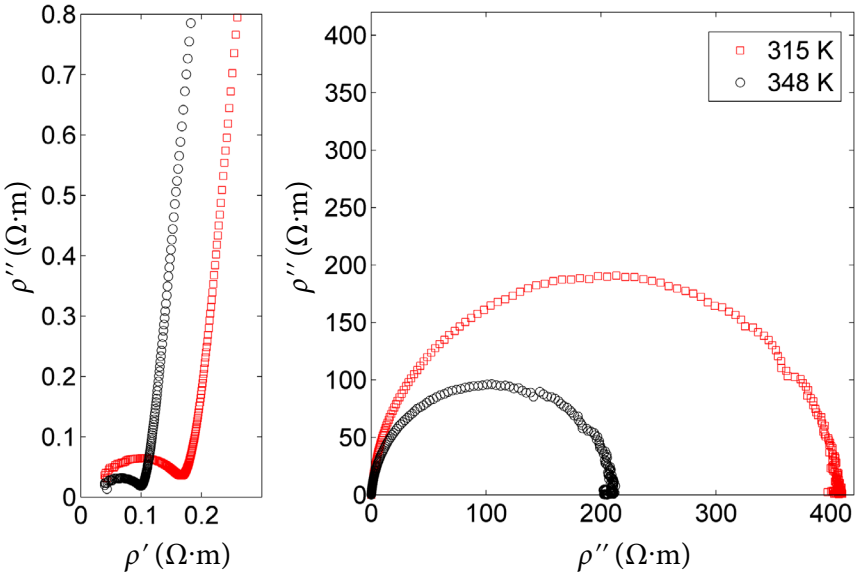

Fig. 5. Nyquist representation of complex resistivity at two selected temperatures. The graph on the lefthand side zooms to the high-frequency range.

The diameters of semicircles correspond to the resistivity values associated to each of the two processes. These values can also be found from the plateau seen in the frequency dependences of the real part of conductivity, hence $\Delta\rho = 1/\sigma'$ (at 1 kHz and at 1 GHz). Temperature dependences of the real part of conductivity at 1 kHz and at 1 GHz are presented in Fig. 6. Both conductivities follow the Arrhenius law

$$\sigma' = \frac{\sigma_0}{T}\exp(-E_A / k_B T), \tag{5}$$

where E_A is the activation energy, σ_0 is the constant, k_B is the Boltzmann's constant, T is the absolute temperature. The activation energies of conductivity were 0.17 and 0.08 eV for the lower frequency relaxation process and for the higher frequency relaxation process, respectively. At 1 GHz and at temperatures higher than ~335 K the increace in the conductivity activation energy can be observed and it may be related with some chemical changes occurring in the Cu_7PS_6 crystal.

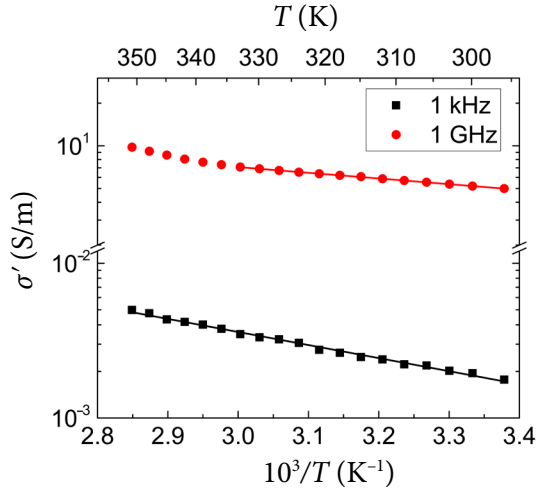

Fig. 6. Arrhenius plot of the real part of conductivity measured at 1 kHz and 1 GHz frequencies. Solid lines are Arrhenius fits.

Two relaxation dispersions observed in the frequency dependences of conductivity can be explained by the presence of several structure non-uniformities (domain boundaries) that create a barrier for charge transfer in the volume of the bulk crystal leading to the low-frequency dispersion region while the high-frequency dispersion is caused by the internal domain capacity and conductivity in this case. The last one is essentially higher (5 S/m) in comparison to the low-frequency value ($1.77\cdot10^{-3}$ S/m) related to charge transfer across the domain boundaries. The presence of domain boundaries associated with growth defects is confirmed by XRD, while orienting the single crystals on the axis closest to the growth direction, and can be caused by higher crystallization velocities and the temperature gradient in the crystallization zone in the Bridgman–Stockbarger technique compared to the chemical vapour transport method used for halogen-containing argyrodites, in which domain boundaries were not found and hence did not contribute to the conductivity spectra [23].

The Cu_7PS_6 crystal is a mixed electronic-ionic conductor with several structure non-uniformities present in it that is confirmed by XRD while orienting the single crystals on the axis closest to

the growth direction. High values of electronic and ionic conductivity make these crystals a perspective electrode material for ionic accumulators and electrochemical sensors.

4. Conclusions

Cu_7PS_6 crystals were grown using direct crystallisation from the melt (Bridgman–Stockbarger technique). The crystal structure of Cu_7PS_6 was determined using the X-ray powder diffraction technique. Cu_7PS_6 are shown to crystallise in the cubic structure, space group $P2_13$ (No. 198), lattice parameter a = 9.6706(1) Å, formula units per all Z = 4, which is identical to β-Cu_7PSe_6.

Electrical parameters of the Cu_7PS_6 crystals were studied in the frequency range 10–10^{10} Hz and the temperature interval 296–351 K. Two processes were observed, which cause two conductivity dispersions and a dielectric dispersion. At room temperature and at 1 kHz frequency the conductivity value is $1.77 \cdot 10^{-3}$ S/m, while at high frequency of 1 GHz the conductivity reaches 5 S/m. The corresponding activation energies of conductivities were found to be 0.17 and 0.08 eV, respectively. Cu^+ ions and electrons/holes contribute to the conductivity in Cu_7PS_6 crystals.

Acknowledgements

This work was financially supported by the Research Council of Lithuania (Project No. TAP-LU-15-005). The authors sincerely thank Prof. Dr. Arno Pfitzner who kindly provided the XRD data.

References

[1] W.F. Kuhs, R. Nitsche, and K. Scheunemann, The argyrodites – a new family of tetrahedrally close-packed structures, Mater. Res. Bull. **14**, 241–248 (1979).

[2] I.P. Studenyak, M. Kranjčec, G.S. Kovacs, I.D. Desnica, V.V. Panko, and V.Yu. Slivka, Influence of compositional disorder on optical absorption processes in $Cu_6P(S_{1-x}Se_x)_5I$ crystals, J. Mater. Res. **16**, 1600–1608 (2001).

[3] I.P. Studenyak, M. Kranjčec, G.S. Kovacs, V.V. Panko, V.V. Mitrovcij, and O.A Mikajlo, Structural disordering studies in $Cu_{6+\delta}PS_5I$ single crystals, Mater. Sci. Eng. B **97**, 34–38 (2003).

[4] A. Gagor, A. Pietraszko, and D. Kaynts, Diffusion paths formation for Cu^+ ions in superionic Cu_6PS_5I single crystals studied in terms of structural phase transition, J. Solid State Chem. **178**, 3366–3375 (2005).

[5] E. Gaudin, F. Boucher, V. Petricek, F. Taulelle, and M. Evain, Structures and phase transitions of the A_7PSe_6 (A = Ag, Cu) argyrodite-type ionic conductors. II. β- and γ-Cu_7PSe_6, Acta Cryst. B **56**, 402–408 (2000).

[6] R.B. Beeken, C.R. Driessen, B.M. Hinaus, and D.E. Pawlisch, Electrical conductivity of Ag_7PSe_6 and Cu_7PSe_6, Solid State Ionics **179**, 1058–1060 (2008).

[7] K.S. Weldert, W.G. Zeier, T.W. Day, M. Panthofer, G.J. Snyder, and W. Tremel, Thermoelectric transport in Cu_7PSe_6 with high copper ionic mobility, J. Am. Chem. Soc. **136**, 12035–12040 (2014).

[8] R.B. Beeken and B.M. Hinaus, The effect of sulfide substitution in the mixed conductor Cu_7PSe_6, J. Phys. Chem. Solids **72**, 1081–1084 (2011).

[9] H. Andrae and R. Blachnik, Metal sulphide-tetraphosphorusdekasulphide phase diagrams, J. Alloys Compd. **189**, 209–215 (1992).

[10] S. Fiechter and E. Gmelin, Thermochemical data and phase transition of argyrodite-type ionic conductors Me_6PS_5Hal and Me_7PS_6 (Me = Cu, Ag; Hal = Cl, Br, I), Thermochim. Acta **87**, 319–334 (1985).

[11] A. Kežionis, E. Kazakevičius, T. Šalkus, and A.F. Orliukas, Broadband high frequency impedance spectrometer with working temperatures up to 1200 K, Solid State Ionics **188**, 110–113 (2011).

[12] A. Kezionis, S. Kazlauskas, D. Petrulionis, and A.F. Orliukas, Broadband method for the determination of small sample's electrical and dielectric properties at high temperatures, IEEE Trans. Microw. Theory Tech. **62**, 2456–2461 (2014).

[13] H.M. Rietveld, A profile refinement method for nuclear and magnetic structures, J. Appl. Crystallogr. **2**, 65–71 (1969).

[14] L.B. McCusker, R.B. Von Dreele, D.E. Cox, D. Louër, and P. Scardi, Rietveld refinement guidelines, J. Appl. Crystallogr. **32**, 36–50 (1999).

[15] A. Altomare, C. Cuocci, C. Giacovazzo, A. Moliterni, R. Rizzi, N. Corriero, and A. Falcicchio, *EXPO2013*: a kit of tools for phasing crystal structures from powder data, J. Appl. Crystallogr. **46**, 1231–1235 (2013).

[16] M. Evain, E. Gaudin, F. Boucher, V. Petricek, and F. Taulellec, Structures and phase transitions of the A_7PSe_6 (A = Ag, Cu) argyrodite-type ionic conductors. I. Ag_7PSe_6, Acta Crystallogr. B **54**, 376–383 (1998).

[17] F. Pertlik, Hydrothermal synthesis and crystal structure determination of heptasilver(I)-disulfur-tetrathioarsenate(V), $Ag_7S_2(AsS_4)$, with a survey on thioarsenate anions, J. Solid State Chem. **112**, 170–175 (1994).

[18] J. Rodriguez-Carvajal, *FullProf.2k: A Rietveld Refinement and Pattern Matching Analysis Program*, Version 5.60 (Laboratoire Léon Brillouin (CEA-CNRS), France, 2015).

[19] R.A. Young and D.B. Wiles, Profile shape functions in Rietveld refinements, J. Appl. Crystallogr. **15**, 430–438 (1982).

[20] J.-F. Bérar and G. Baldinozzi, Modeling of line-shape asymmetry in powder diffraction, J. Appl. Crystallogr. **26**, 128–129 (1993).

[21] W.A. Dollase, Correction of intensities for preferred orientation in powder diffractometry: application of the March model, J. Appl. Crystallogr. **19**, 267–272 (1986).

[22] E. Jansen, W. Schäfer, and G. Will, R-values in analysis of powder diffraction data using Rietveld refinement, J. Appl. Crystallogr. **27**, 492–496 (1994).

[23] I.P. Studenyak, M. Kranjčec, V.V. Bilanchuk, O.P. Kokhan, A.F. Orliukas, A. Kezionis, E. Kazakevicius, and T. Salkus, Temperature variation of electrical conductivity and absorption edge in Cu_7GeSe_5I advanced superionic conductor, J. Phys. Chem. Solids **70**, 1478–1481 (2009).

ARGIRODITO TIPO Cu_7PS_6 KRISTALŲ STRUKTŪRA IR ELEKTRINĖS SAVYBĖS

I.P. Studenyak [a], V.Yu. Izai [a], A.I. Pogodin [a], O.P. Kokhan [a], V.I. Sidey [a], M.Yu. Sabov [a], A. Kežionis [b], T. Šalkus [b], J. Banys [b]

[a] *Užhorodo nacionalinis universitetas, Užhorodas, Ukraina*

[b] *Vilniaus universiteto Fizikos fakultetas, Vilnius, Lietuva*

Santrauka

Cu_7PS_6 kristalai užauginti iš lydalo pagal Bridžmeno ir Stokbargerio schemą. Cu_7PS_6 kristalų struktūra ištirta atlikus rentgeno spindulių difrakcijos matavimus. Nustatyta, kad šis junginys kristalizuojasi kaip kubinės singonijos kristalas (erdvinė simetrijos grupė – $P2_13$, elementariosios kristalinės gardelės parametras a = 9,6706(1) Å). Elektrinės kristalo savybės tirtos impedanso spektroskopijos metodu 10–10^{10} Hz dažnių diapazone ir 296–351 K temperatūrų intervale. Stebėti du relaksaciniai procesai, kurie lėmė dvi elektrinio laidumo ir aiškiai išreikštą dielektrinę dispersijas. Esant kambario temperatūrai žemųjų dažnių srityje (1 kHz) išmatuotas elektrinis laidumas yra 1,77 · 10^{-3} S/m, o aukštuosiuose dažniuose (1 GHz) elektrinio laidumo vertė siekia 5 S/m. Atitinkamos šių laidumų aktyvacijos energijos yra 0,17 ir 0,08 eV. Cu_7PS_6 kristale krūvio pernašoje dalyvauja Cu^+ jonai ir elektronai / skylutės.